

Insights and Implications of Intricate Surface Charge Transfer and sp^3 -Defects in Graphene/Metal Oxide Interfaces

Daria Belotcerkovtceva, Renan P. Maciel, Elin Berggren, Ramu Maddu, Tapati Sarkar, Yaroslav O. Kvashnin, Danny Thonig, Andreas Lindblad, Olle Eriksson, and M. Venkata Kamalakar*



Cite This: *ACS Appl. Mater. Interfaces* 2022, 14, 36209–36216



Read Online

ACCESS |



Metrics & More



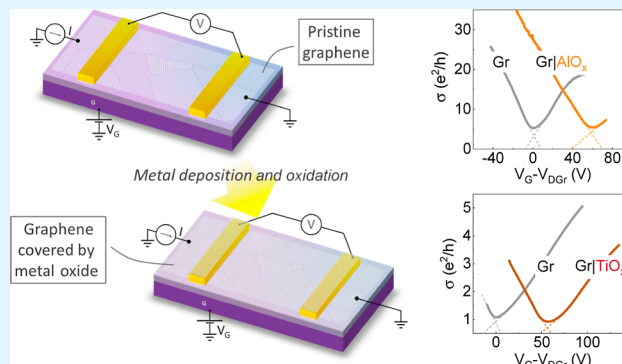
Article Recommendations



Supporting Information

ABSTRACT: Adherence of metal oxides to graphene is of fundamental significance to graphene nanoelectronic and spintronic interfaces. Titanium oxide and aluminum oxide are two widely used tunnel barriers in such devices, which offer optimum interface resistance and distinct interface conditions that govern transport parameters and device performance. Here, we reveal a fundamental difference in how these metal oxides interface with graphene through electrical transport measurements and Raman and photoelectron spectroscopies, combined with *ab initio* electronic structure calculations of such interfaces. While both oxide layers cause surface charge transfer induced p-type doping in graphene, in sharp contrast to TiO_x , the AlO_x /graphene interface shows the presence of appreciable sp^3 defects. Electronic structure calculations disclose that significant p-type doping occurs due to a combination of sp^3 bonds formed between C and O atoms at the interface and possible slightly off-stoichiometric defects of the aluminum oxide layer. Furthermore, the sp^3 hybridization at the AlO_x /graphene interface leads to distinct magnetic moments of unsaturated bonds, which not only explicates the widely observed low spin-lifetimes in AlO_x barrier graphene spintronic devices but also suggests possibilities for new hybrid resistive switching and spin valves.

KEYWORDS: graphene, charge transfer, graphene electronics, spintronics, sp^3 -defects



INTRODUCTION

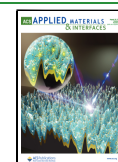
Graphene has evolved into an ideal medium for quantum and spin transport applications and a unique integration platform for complex heterostructures with other two-dimensional (2D) materials.^{1,2} Recent developments show record quantum and spin transport performance that can be achieved in large-scale chemical vapor deposited (CVD) graphene, making it a prospective material for practical implementation into quantum and spin-integrated circuits.^{3–5} Metal oxide interfaces are integral to graphene nanoelectronics and spintronic devices, ranging from memristors and single-electron transistors to tunnel field-effect transistors and graphene spin valves, where the interface nature guides their performance. In particular, titanium oxide and aluminum oxide have been widely used as tunnel barriers, primarily due to their efficacy and compatibility with device processing methods. Although ultrathin metal oxide layers can be directly realized using atomic-layer deposition or sputtering techniques, these techniques can lead to significant defects, impacting the overall structure and electrical nature of graphene.^{6,7} Instead, Ti and Al are deposited using electron beam evaporation in graphene spin devices and are subsequently oxidized upon contact with air/ O_2 . In graphene electronic devices, metal oxides are used as gate dielectrics, effective barriers for graphene tunnel

junctions,⁸ and thin-film memristive devices⁹ for practical imitation of synaptic activities, where interface charge transfer and bonding can guide the resistive switching phenomena.¹⁰ For both planar and vertical graphene spintronic devices,^{11,12} ultrathin layers (\sim nm thickness) of the metal oxides serve as tunnel barriers offering optimum interface resistance to overcome the conductivity mismatch problem associated with electrical spin injection.^{13,14} However, obtaining faithful pinhole-free coverage is challenging for both aluminum and titanium oxides, prepared by e-beam metal evaporation and post-oxidation. In particular, compared to spin lifetimes up to ~ 3.5 ns in graphene spintronic devices using TiO_x barriers,^{15–17} the AlO_x -based devices widely show an order lower spin lifetime of ~ 100 ps,^{18–20} which has been generally attributed to the presence of pinholes, consequent current crowding, and contact-induced spin relaxation.^{21,22} The one order lower performance of AlO_x -based devices remains

Received: April 14, 2022

Accepted: June 29, 2022

Published: July 22, 2022



puzzling, despite the same fabrication process and similar thicknesses of oxides. Therefore, understanding the physics governing graphene/metal-oxide interfaces is of fundamental significance to graphene nanoelectronic and spintronic devices. While metals and metal oxides on graphene introduce surface charge transfer p-type or n-type doping arising from the difference in the work function of the metal relative to graphene,^{17,23,24} the situation is non-trivial for tunnel barrier oxides such as ultrathin TiO_x or AlO_x on graphene. Considering expected charge transfer effects, the redistribution of electron density after oxidation of metals is unclear, even from a theoretical perspective. In addition to surface charge-transfer doping, in-plane and out-of-plane defect-related doping in graphene can greatly influence charge and spin relaxation. The possibilities of introducing long-range and short-range scatterers, defects due to ultrathin oxide layers on graphene, and their direct influence on electrical properties of graphene and spin relaxation in tunnel transport through such barriers have never been explicit. This investigation aims to uncover, at an atomic level, the important differences in the nature of defects between Al oxide and Ti oxide adhering to graphene for their influence on electrical and spintronic performance.

MATERIALS AND METHODS

In this work, we explore the modifications in graphene due to its full coverage with metal oxides through electrical transport measurements, spectroscopic techniques, atomic force microscopy, and theoretical electronic structure calculations. To faithfully explore the extrinsic doping, defect effects, and their implications, we investigated the impact of TiO_x and AlO_x adsorption on the electronic properties of fully covered graphene. To understand the electronic alterations due to oxides, we measured electrical properties on the same devices before and after the oxide realization by metal deposition and oxidation. X-ray photoelectron spectroscopy (XPS) and Raman spectroscopy were used to determine the nature of doping and oxidation states of C, Al, and Ti in AlO_x- and TiO_x-covered graphene and their distinct interface behavior. The topography, probed by atomic force microscopy (AFM), shows characteristic features and coverage unique to each kind of oxide. We correlate these results with electronic structure calculations to understand the intricate interfacial properties and possible atomic and electronic configurations that lead to our experimental observations. Finally, we discuss how the interface defects observed in this study illuminate the current understanding of spin relaxation in the widely used tunnel barriers in graphene spintronics and lead to new implications for nanoelectronic and spintronic devices.

Figure 1 shows graphene field-effect devices used in our experiments before and after metal (metal oxide) realization on graphene. The first step in fabricating graphene devices is to pattern a graphene channel using optical lithography and Ar plasma etching, resulting in 5 μm wide graphene stripes. Following this, graphene devices were fabricated by electron beam lithography patterning, e-beam metal evaporation, and subsequent lift-off (details in the Supporting Information). Next, electrical measurements were performed on the resulting devices to obtain transport parameters of the pristine graphene channels. After these initial measurements, the devices were subjected to an additional layer of metal oxide by electron beam evaporation and oxidation in open air. The critical part of the procedure is the Ti or Al (0.8 nm) deposition on the same device and keeping the device working for repeated measurements with the metal oxide layers on top of graphene. This allowed us to understand the modification due to doping and possible defect creation in the same graphene stripes.

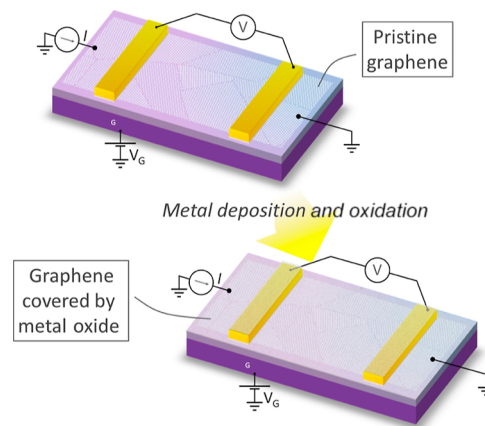


Figure 1. Experimental scheme of a graphene field-effect device before and after Al/Ti deposition and oxidation.

RESULTS AND DISCUSSION

The initial characterization of changes in the graphene properties was carried out by gate-dependent measurements of four-probe channel sheet-resistance (R_{\square}) with varying gate voltage (V_G). To determine the contribution stemming from graphene and graphene covered with TiO_x/AlO_x, Dirac curves were measured on the same devices before and after the deposition of the metals. As shown in Figure 2a,b, for both oxide layers, the charge neutrality point (CNP), that is, the Dirac point (V_D), shifts toward the positive gate voltage region. Such a shift means that these metal oxides cause a downward shift of the Fermi level in graphene, implying p-type doping. It is worth noting that the V_D shift (ΔV_D) is significant even with an ultrathin ~1 nm layer, and the interface trap density of states for the acceptor is affected by both types of oxides, as evidenced by ΔV_D . In Figure 2c–j, all electrical parameters are compared with pristine graphene to determine changes in a total of 12 devices measured here. Despite the huge variation in V_D (i.e., doping level), minimum conductivity (σ_0), and mobility (μ), both oxide-overlaid graphene samples show reasonably good values, and for most of the devices, the changes are moderately small (similar to or ~10% for most devices) from initial pristine graphene devices to graphene/oxide devices. Strikingly, the sheet resistance at the CNP is similar for graphene before and after metal oxide realization, indicating a minimum conductivity that remains reasonably intact (as shown in Figure 2i,j). The minimum conductivity at V_D for both oxides (Figure 2i,j) showed less than 5% change from pristine graphene samples. Furthermore, in the shape of the Dirac curves, the plateaus around the CNP in the metal oxide-covered devices are not appreciably different from those seen in the pristine devices. The analysis of Dirac curves reveals (see Supporting Information Figure S1) a low trap density in all samples, and the minor changes in electrical parameters after the realization of top oxide layers can be linked to modifications in long-range Coulomb scattering due to charged impurities²⁵ and the short-range defect scattering,²⁶ including possible sp³ defects. Considering that Al and Ti metals result in n-type doping in graphene,^{24,27,28} these observations suggest that the p-type doping of ~10¹² to 10¹³ cm⁻² (for change in ΔV_D of ~50–100 V) is primarily due to the surface charge transfer between the oxide layers and graphene for most devices. This means that the oxide layer coverage achieved by electron beam evaporation and

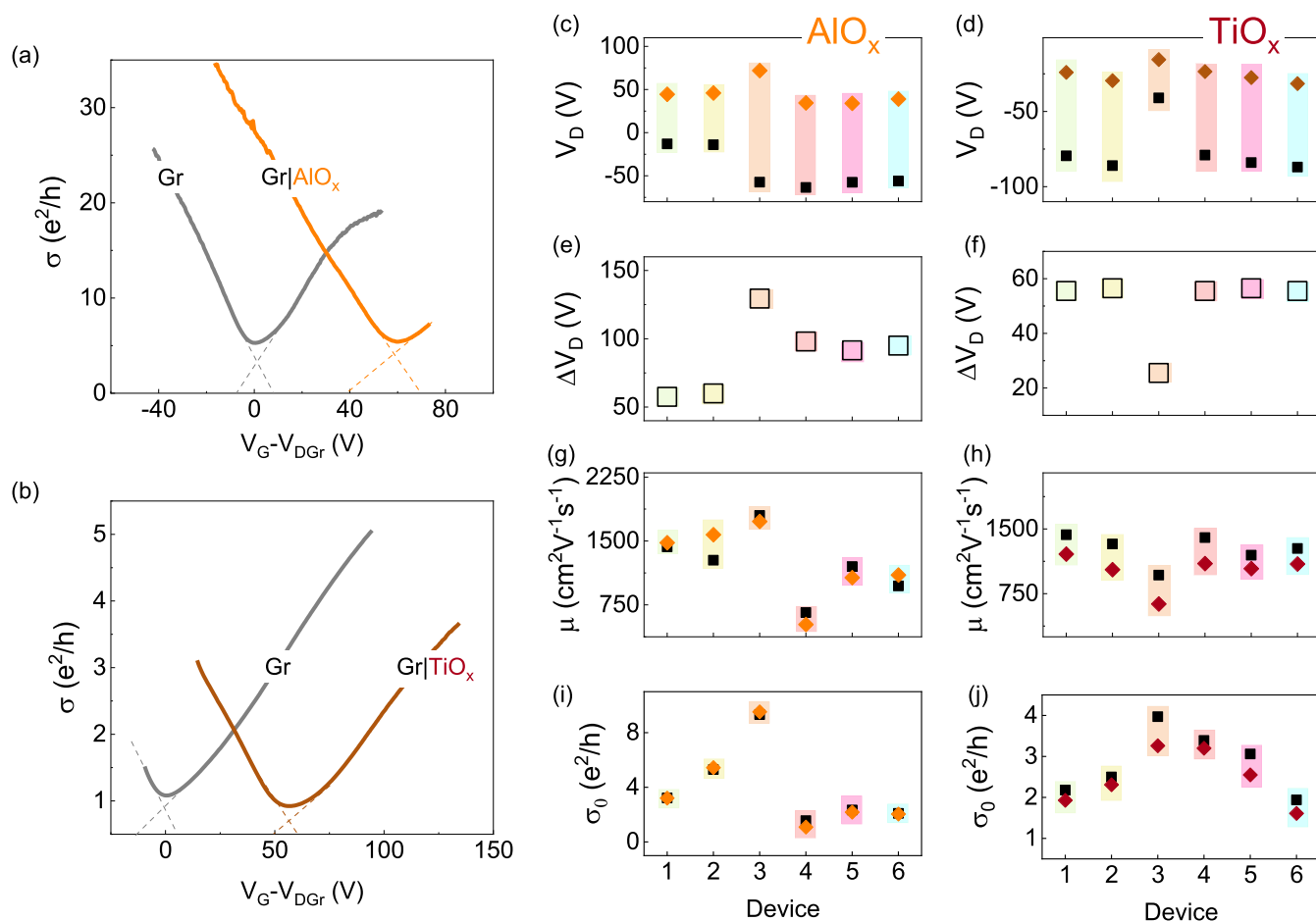


Figure 2. Electrical characteristics' modification for graphene devices with AlO_x and TiO_x layers. Gate-dependent conductivity (in units of quantum of conductance e^2/h) vs gate voltage (V_G). Dirac curves for the devices with graphene before (gray curve) and after (orange/brown curve) deposition of (a) AlO_x and (b) TiO_x . The dashed lines are provided here to guide Dirac point broadening. (c–j) Summary of Dirac point location (V_D) and its shift (ΔV_D), field-effect electron mobility (μ), minimum conductivity (σ_0) for pristine graphene (dark square), and AlO_x - and TiO_x -deposited (colored diamond) devices.

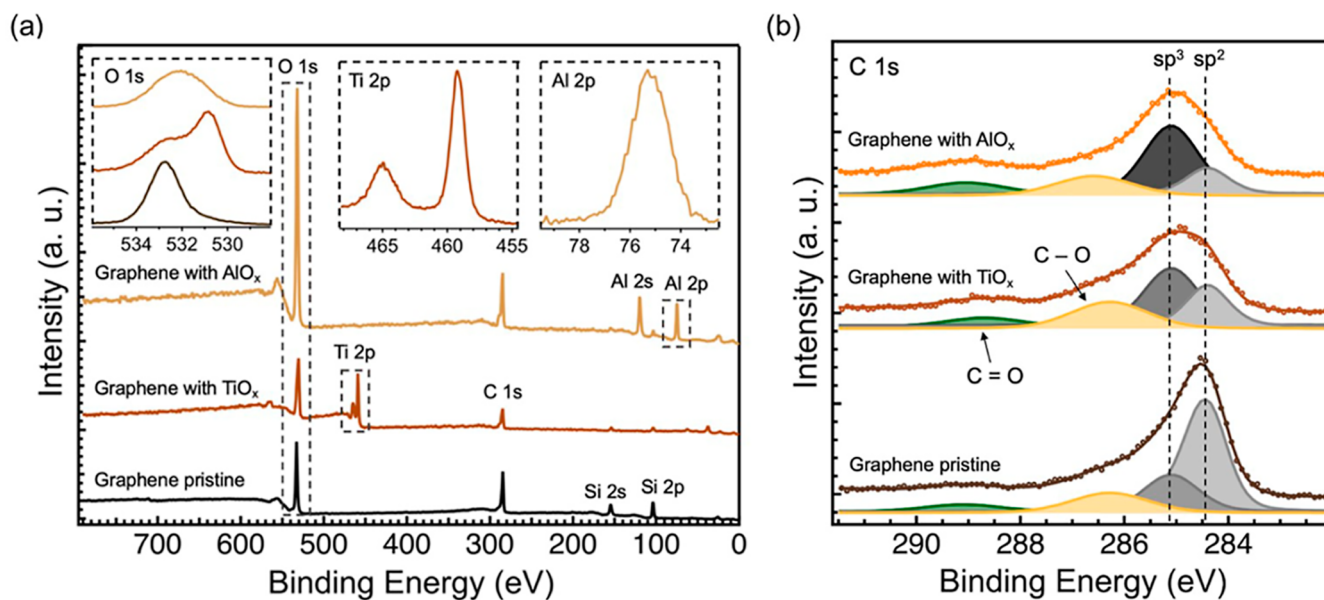


Figure 3. XPS characterization. (a) Overview spectra of pristine graphene (dark brown), graphene with deposited TiO_x (brown), and AlO_x (orange), and (b) C 1s components used for the least-squares fits. All spectra were obtained using a monochromatic Al K_{α} source. The binding energy is calibrated using the Si 2p peak at 103.3 eV in SiO_2 ³⁷ and the carbon sp^2 peak at 284.4 eV.^{38,39}

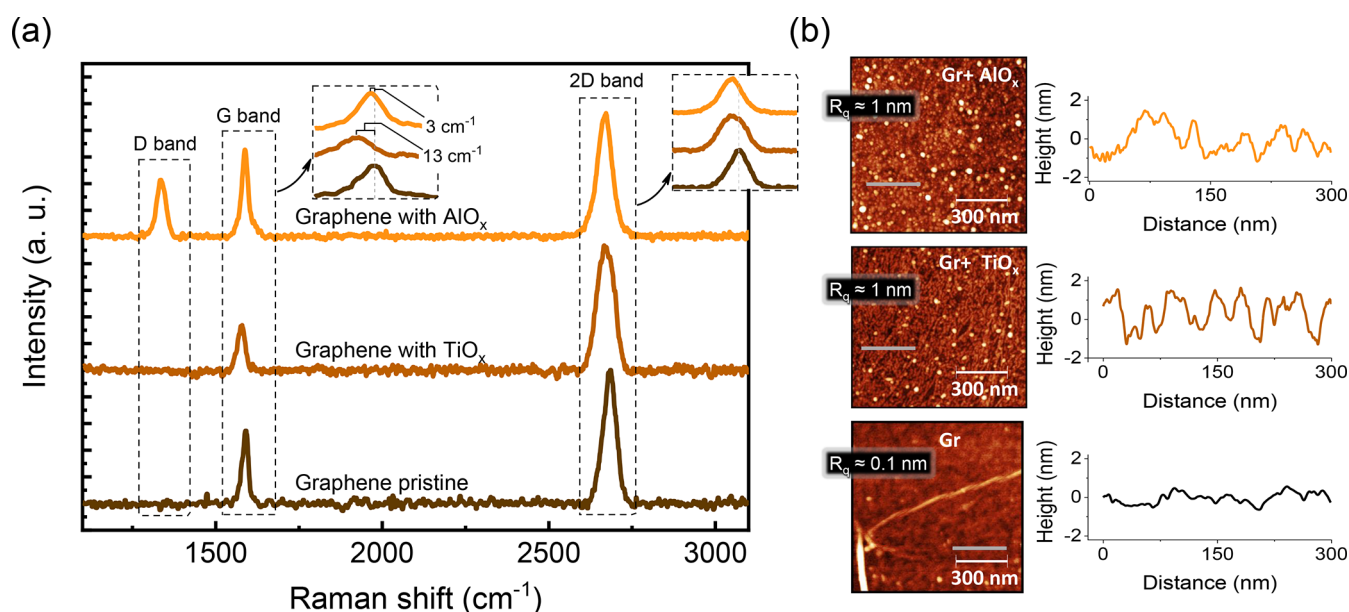


Figure 4. (a) Raman spectra of pristine graphene and graphene with deposited TiO_x and AlO_x along with insets showing shifts in G and 2D bands. (b) AFM images of representative graphene (Gr) and graphene after TiO_x (Gr + TiO_x) and AlO_x (Gr + AlO_x) deposition on top of it. The corresponding gray line scans show the roughness profiles, and R_q represents the average area roughness.

subsequent oxidation can be used to protect graphene without drastically altering its properties. The charge transfer serves as a tool to tune the carrier concentration faithfully. It is known that in-plane defects in graphene can lead to n-type doping,²⁹ which rules out such defects. However, in addition to charge-transfer doping, sp^3 out-of-plane defects could also lead to p-type doping³⁰ and can cause spin-flip scattering as well as spin precession relaxation in graphene. To further explore the nature of such defects, we performed XPS measurements (see sample characterization details in the Supporting Information) on our samples.

In Figure 3, the XPS data on pristine graphene and graphene with metal oxide layers are shown. The Al 2p spectrum (Figure 3a, upper right panel) shows a binding energy of 75 eV, suggesting that the deposited film is Al_2O_3 .³¹ The regional spectrum of Ti 2p (Figure 3a, central panel) shows a binding energy of 459 eV for the Ti $2p_{3/2}$ core level, corresponding to TiO_2 .^{32,33} This implies that both metals are nearly fully oxidized. The XPS spectra for C 1s core-level binding energy is shown in Figure 3b. The observed increase in binding energy for oxide-covered samples suggests a charge transfer from graphene to interface atoms, confirming p-type doping. Figure 3b shows that the pristine graphene sample exhibits an expected intense sp^2 contribution compared to graphene covered with metal oxides. The observed background contribution of sp^3 can come from other sources, such as resist residue and other C-species in the sample measurement environment. In sharp contrast, the Gr- AlO_x sample shows a dominating contribution from sp^3 defects (intensity ratio of $\text{sp}^3/\text{sp}^2 \approx 3$), which signals strong evidence of sp^3 defects created in the graphene lattice during the Al oxidation. Conversely, the transport parameters suggest that sp^2 contribution should maintain dominance even for Gr- AlO_x , so significant quenching of the signal of sp^2 contribution can be due to the added surface oxide layers. Unlike Gr- AlO_x samples, we observe a lower value of $\text{sp}^3/\text{sp}^2 \approx 1.6$ for Gr- TiO_x , suggesting a lower-level source of the sp^3 signal. Here, in our analysis, subtracting the sp^3 contributions of bare graphene

from our oxide samples can reveal some sp^3 contribution also in Gr-metal oxide samples. However, since each sample has its own background, for comparisons, we chose to look at the sp^3/sp^2 intensity ratios. Considering that high spin lifetimes were achieved with TiO_x tunnel barriers, the increased sp^3 intensity does not necessarily mean an sp^3 hybridization of the graphene lattice.³⁴ In fact, with a large $100 \mu\text{m}$ X-ray probe diameter, a significant sp^3 contribution can originate from the PMMA resist residues and related effects intrinsic to the CVD graphene transfer process^{35,36} (similar to the sp^3 background in pristine graphene). This, and the possible reduction in sp^2 intensity due to oxide coverage, could increase the observed intensity at the sp^3 binding energy for Gr- TiO_x . Additionally, it is worth noting that surface carbon species bonded to oxygen atoms can have binding energies equivalent to those of sp^3 -carbon,³⁴ which could further add to the surplus intensity at the sp^3 -binding energy position for the Gr- TiO_x sample. Thus, the XPS measurements with large-area sampling give qualitative evidence of the presence of sp^3 carbon in the graphene lattice covered with AlO_x . On the other hand, large-area sampling can be circumvented by micro-Raman characterization. Figure 4 shows the Raman spectra obtained on pristine graphene and graphene with metal oxide layers. First, as shown in Figure 4, for pristine graphene, the well-known G and 2D mode features, with frequencies near 1584 and 2678 cm^{-1} , respectively, were obtained. The same peaks were also identified on the graphene samples with AlO_x or TiO_x layers, confirming the integrity of graphene sheets covered by oxide layers.

The ratio of the 2D peak to the G peak intensities (I_{2D}/I_G) is a parameter to determine the quality and monolayer structure of graphene.⁴⁰ Here, in pristine graphene and graphene with TiO_x , $I_{2D}/I_G \geq 2$ confirms the good quality of the CVD polycrystalline graphene that we employed in this study.⁴¹ However, in the presence of AlO_x , graphene shows different behavior, with the value of I_{2D}/I_G significantly decreasing to 1.45, which suggests possible degradation of the sp^2 structure of graphene. In addition, the G peak's doping sensitivity helps

confirm the nature of doping. The location of the G peak for pristine graphene is 1590 cm^{-1} . For graphene coated with AlO_x , the peak shift was approximately 3 cm^{-1} and for the case of TiO_x , it was approximately 13 cm^{-1} compared with pristine graphene. A similar shift was also observed for the 2D peak. Such a Raman shift to the left in the oxide-layered graphene indicates a p-type doping effect, which is in good agreement with our transport and XPS measurements. However, in the case of aluminum oxide-covered graphene, strikingly, we observed the emergence of the D peak (near 1340 cm^{-1}), which is a signature of Raman-active defects in graphene, suggesting the introduction of appreciable sp^3 carbon defects, a source of graphene modification by AlO_x only. Although Raman spectroscopy in most cases serves as a qualitative analysis, it is possible to quantify the presence of defects in graphene. Using the model proposed in literature,⁴² we obtained the concentration of defects for a graphene sample with AlO_x by extracting the G to D intensity ratio from the spectrum and the excitation laser wavelength (see Raman spectroscopy details in the Supporting Information). From the estimation, we found a concentration of defects for graphene with evaporated Al (0.8 nm) of $\sim 1.4 \times 10^{11}\text{ cm}^{-2}$, which is nearly one defect per 10,000 carbon atoms. As stated earlier, for a large shift in V_D of $\sim 50\text{--}100\text{ V}$, a corresponding doping of 10^{12} to 10^{13} cm^{-2} can be expected. Therefore, the significant doping is due to surface charge-transfer doping, while the sp^3 -related defect contributions are up to 2 orders less, which is unique to the AlO_x -interfaced graphene. Despite the defects, the electrical properties of graphene are relatively preserved in graphene/ AlO_x devices. In graphene spintronic devices, the sp^3 defects are expected to contribute to spin relaxation, mainly when the electrical spin injection is carried out in graphene spintronic devices, resulting in significantly shorter spin lifetimes. This has been conventionally attributed to pinholes in the AlO_x barrier. Density functional theory (DFT)-based electronic structure calculations showed that the interaction between graphene and metal oxides is weaker for Ti oxide than for Al oxide.⁴³ The Ti-donated electron charge density is highly localized around the neighboring carbon atoms, and titanium does not tend to form clusters, which is expected to lead to uniform coverage.⁴⁴ To understand the surface morphology of the oxide coverage over graphene, we investigated the samples by AFM. We chose a $1\text{ }\mu\text{m} \times 1\text{ }\mu\text{m}$ scan area to check the shape of the grains on top of the graphene surface and the height profile. Expectedly, there is a deviation from the smooth morphology of pristine graphene to graphene with the oxide layers. The common feature of oxide-covered graphene is the presence of ridges and grooves. The comparison between the surfaces is shown in Figure 4b. The AFM images show an alternation of dark and bright stripes in the case of Ti or circle-shaped dots in Al. The mean position was fixed to a 0 nm height in the height profile. Compared to the height profile with the standard topography of graphene, the oxide-covered graphene possesses a higher topographic root-mean-square roughness. While conspicuous pinholes can be identified from the deviation in the height profile and images for AlO_x , perceptible swings in the height profile are also observed in the Gr- TiO_x system. One can attribute the other large clusters to possible resist residue regions observed in pristine graphene that can act as nucleation sites. Both oxides show an area roughness of $R_q \sim 1\text{ nm}$, suggesting that both Ti and Al deposited on graphene by e-beam evaporation and following oxidation of the metals do not necessarily lead to

full coverage, and hence, current crowding can be a common problem for both metal oxides. This leaves us with the additional sp^3 defects unique to AlO_x -layered graphene. Despite the XPS data indicating that Al and Ti are fully oxidized, we cannot assure perfect stoichiometric compositions leading to the observed charge-transfer doping in graphene. In particular, previous DFT calculations established charge transfer from graphene to titanium.^{45,46} However, the charge transfer and sp^3 defect interface in graphene-Al oxide have not been addressed. To understand that on an atomic scale, we performed electronic structure calculations, shown in Figure 5.

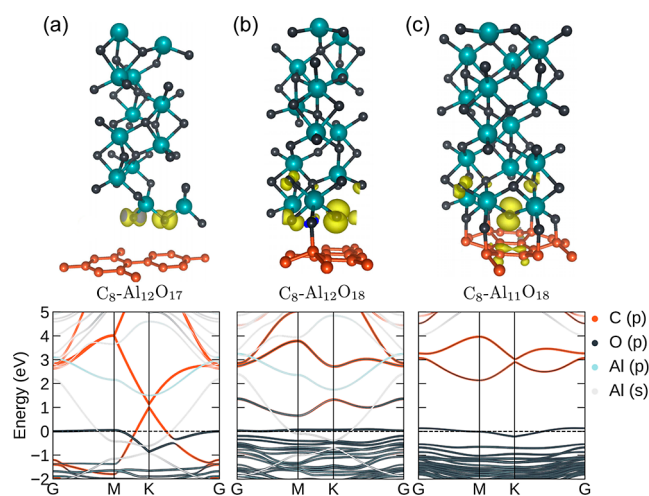


Figure 5. Simulated system's geometry (upper panel). The atoms Al, O, and C are represented by green, gray, and orange, respectively. The yellow clouds are the atom-projected magnetic moment densities of the crystal. The lower panel shows the projected band structure of (a) slightly off-stoichiometric aluminum oxide on graphene monolayer structures ($\text{C}_8\text{-Al}_{12}\text{O}_{17}$): the Fermi level shifts down in relation to the Dirac point and the unit cell magnetic moment is $\sim 0.44\text{ }\mu_B$. (b) Perfect stoichiometry ($\text{C}_8\text{-Al}_{12}\text{O}_{18}$) giving rise to partially sp^3 -bonded graphene leading to a local band gap opening and magnetic moments ($0.61\text{ }\mu_B$ per unit cell). (c) Electronic structure of graphene with sp^3 -bonded $\text{C}_8\text{-Al}_{11}\text{O}_{18}$ where the unit cell magnetic moment is $1\text{ }\mu_B$. The s- and p-bands from Al crossing both the Dirac cone and Fermi level (gray colored bands) are due to dangling bonds at the very top surface of the composite.

Taking experimental conditions into account and using DFT calculations, we performed an interface study of the AlO_x corundum α -phase with a hexagonal unit cell in contact with a graphene monolayer sheet. The AlO_x slab structure can be arranged with different atomic terminations in proximity to graphene (e.g., oxygen or aluminum atom). Each case leads to varying results of the electronic property of the composite. Here, we only highlight three different interfaces (i.e., $\text{C}_8\text{-Al}_{12}\text{O}_{18}$, $\text{C}_8\text{-Al}_{11}\text{O}_{18}$, and $\text{C}_8\text{-Al}_{12}\text{O}_{17}$) where oxygen is in proximity to graphene and the total energy suggests stable or metastable geometries. For all cases, the geometry was relaxed following force minimization. For other geometries and details, see the Supporting Information. Figure 5 shows atomic and electronic structure results for AlO_x layers on graphene using the experimental oxide layer thickness value of $\sim 1\text{ nm}$. Notably, calculations performed for the perfect stoichiometry ($\text{C}_8\text{-Al}_{12}\text{O}_{18}$), with graphene interfaced with aluminum atoms, did not yield any charge transfer and the Fermi level remained intact (see the Supporting Information). However, when oxygen atoms are in proximity to graphene, a strong

hybridization between the p-orbitals from oxygen and p_z -orbitals from carbon atoms causes the Dirac cone to be strongly distorted and positioned above the Fermi level.

Interestingly, calculations with a slight off-stoichiometry ($\text{Al}_{12}\text{O}_{17}$) give rise to systematic Fermi-level shifts of ~ 1 eV and p-doping with oxygen atoms closer to the graphene lattice (Figure 5a) without completely distorting or destroying the Dirac cone. In the process of e-beam evaporation of Al, the possibility of Al atoms scattered from the graphene lattice and the activated carbon atoms being susceptible to subsequent bonding with oxygen atoms cannot be ruled out. Our calculations suggest that oxygen atoms can also make sp^3 bonds with graphene, as shown in Figure 5b,c. The calculations reveal that p-type doping emerges due to the oxygen atoms next to the graphene layer. However, for stoichiometric and slightly off-stoichiometric Al_2O_3 , even a few oxygen atoms firmly bound with the carbon atoms buckle the graphene layer locally and destroy the Dirac cone by inducing sp^3 states and a local band gap opening. For computational reasons, the number of sp^3 defects considered in the calculations is relatively high compared to experiments (where 1 out of 10,000 atoms have Raman-active sp^3 defects). Nevertheless, the presented calculations show how sp^3 bonds can induce significant band gap opening. The practical scenario for our samples prepared with CVD graphene can combine these two features with every 10,000th location featuring a band structure as in Figure 5c. Overall, our experiments reveal that sp^3 -hybridized defect centers are a significant feature of AlO_x , which is expected to buckle graphene locally. Such buckling is known to introduce spin-orbit coupling⁴⁷ and magnetic moments.⁴⁸ Our calculations with both perfect stoichiometric and non-stoichiometric Al-oxide sp^3 -bonded systems lead to an effective magnetic moment situated on unsaturated bonds, with values ranging from $0.44 \mu_B$ (off-stoichiometric) to $1 \mu_B$ (high-density sp^3 -bonded lattice) per unit cell.

In this investigation, we observed that non-invasive e-beam-evaporated Al and Ti-based oxides with metals near full-oxidized states adhere in subtle ways to graphene. While both oxides cause surface charge-transfer doping, the sp^3 defects at the graphene/ AlO_x interface can have significant implications for graphene spintronics, where spin currents are injected from a ferromagnet into graphene through the ultrathin oxide barrier. Spin-orbit coupling and local magnetic moments can dominate spin-flip and resonant scattering at graphene/ AlO_x interfaces. Specifically, the resonant scattering with magnetic impurities has been considered responsible for observing low spin lifetimes of ~ 100 ps, widely observed in AlO_x barrier graphene spintronic devices.⁴⁹ With no magnetic ordering, the sparsely distributed sp^3 -based magnetic moments can become an additional source of spin relaxation in AlO_x barrier-based devices, other than the previously attributed pinholes in Al-oxide barrier-based studies in graphene spintronics. Furthermore, our calculations show that despite these magnetic moments being predominantly concentrated at non-saturated bonds (as shown in Figure 5), they can nevertheless induce magnetization in a small region of the graphene sheet, implying a significant source of spin scattering at the interface. In graphene spintronics, although hydrogenated graphene displayed increased spin lifetime with a normal g-factor,⁵⁰ enhanced spin-scattering due to magnetic moment formation in graphene⁵¹ and reduced spin lifetimes due to colossal spin-orbit coupling⁵² have also been reported. Therefore, spin transport experiments with aluminum oxide-covered graphene

could provide further insights into such observations. At the same time, the sparse magnetic moments at graphene/ AlO_x interfaces could be ordered in exotic heterostructures via proximity effects¹¹ for enhanced proximity-induced magnetism in graphene^{11,53} and in a controlled manner for novel spin valves. For resistive switching devices, the sp^3 bonds can act as carrier traps for synaptic junctions, and oxygen ions in the AlO_x layer can be highly mobile in graphene and could form covalent bonds with the broken bonds of graphene for setting and resetting processes in memristive devices.¹⁰ Thus, magnetic defects with exchange-biased layers show potential for hybrid multilevel spin valve-resistive switching random access memory devices.

CONCLUSIONS

In summary, we explored the subtle nature of ultrathin Al and Ti oxides interfacing with graphene. With similar coverage observed by AFM, electrical measurements revealed surface charge transfer p-type doping of $\sim 10^{12}$ to 10^{13} cm^{-2} for both metal oxides, with reasonably preserved charge mobility and sheet resistance. However, X-ray photoelectron spectroscopy suggests an intricate nature of the doping, not just due to charge transfer from C-atoms but also due to significant sp^3 defects for Al-oxide. This is precisely confirmed by the emergence of the sp^3 defect-active Raman D band for Al-oxide-layered graphene, in sharp contrast to Ti-oxide-layered graphene, where the band was absent. Our electronic structure calculations suggest that the observed 100 ppm sp^3 defects originate from O bonding with C and an out-of-plane buckling of carbon atoms. Such defects in Al-oxide-layered graphene can lead to a local magnetic moment in ~ 0.5 – $1.0 \mu_B$, primarily located on unsaturated bonds of O atoms. In the Ti-oxide case, this moment is absent, which offers an explanation for the dramatic difference in spin lifetimes widely observed in devices with different oxide tunnel contacts. At the same time, these results provide new implications for developing unique interfaces for hybrid graphene resistive switching and spintronic devices.

ASSOCIATED CONTENT

Supporting Information

The Supporting Information is available free of charge at <https://pubs.acs.org/doi/10.1021/acsami.2c06626>.

Details of the device fabrication process; sample characterization using electrical measurements and analysis, Raman spectroscopy, AFM, and X-ray photoelectron spectroscopy; and computation details for aluminum oxide simulation with aluminum oxide interface construction, perfect stoichiometric AlO_x /graphene interface, a small concentration of sp^3 bond in perfect stoichiometric oxide, and slightly off-stoichiometric AlO_x /graphene interface (PDF)

AUTHOR INFORMATION

Corresponding Author

M. Venkata Kamalakar – Department of Physics and Astronomy, Uppsala University, SE-751 20 Uppsala, Sweden; orcid.org/0000-0003-2385-9267; Email: venkata.mutta@physics.uu.se

Authors

- Daria Belotckerkovtceva – Department of Physics and Astronomy, Uppsala University, SE-751 20 Uppsala, Sweden
- Renan P. Maciel – Department of Physics and Astronomy, Uppsala University, SE-751 20 Uppsala, Sweden
- Elin Berggren – Department of Physics and Astronomy, Uppsala University, SE-751 20 Uppsala, Sweden
- Ramu Maddu – Department of Materials Science and Engineering, Uppsala University, SE-751 03 Uppsala, Sweden
- Tapati Sarkar – Department of Materials Science and Engineering, Uppsala University, SE-751 03 Uppsala, Sweden; orcid.org/0000-0003-4754-2504
- Yaroslav O. Kvashnin – Department of Physics and Astronomy, Uppsala University, SE-751 20 Uppsala, Sweden
- Danny Thonig – Department of Physics and Astronomy, Uppsala University, SE-751 20 Uppsala, Sweden; School of Science and Technology, Örebro University, SE-70182 Örebro, Sweden
- Andreas Lindblad – Department of Physics and Astronomy, Uppsala University, SE-751 20 Uppsala, Sweden; orcid.org/0000-0002-9188-9604
- Olle Eriksson – Department of Physics and Astronomy, Uppsala University, SE-751 20 Uppsala, Sweden; School of Science and Technology, Örebro University, SE-70182 Örebro, Sweden

Complete contact information is available at:
<https://pubs.acs.org/10.1021/acsami.2c06626>

Notes

The authors declare no competing financial interest.

ACKNOWLEDGMENTS

We gratefully acknowledge funding from the European Research Council (ERC) Project SPINNER, Swedish Research Council (VR starting grants 2016-03278, 2017-05030, 2019-03666, and 2019-03569 as well as project grant 2021-03675), Stiftelsen Olle Engkvist Byggmästare (200-0602), Energimyndigheten (48698-1), Formas (grant no. 2019-01326), Wenner-Gren Stiftelserna (UPD2018-0003 and UPD2019-0166), and Göran Gustafsson Foundation (grant no. 2132). M.V.K. and D.B. thank Olof Karis and José M. Caridad for helpful discussions.

REFERENCES

- (1) Fiori, G.; Bonaccorso, F.; Iannaccone, G.; Palacios, T.; Neumaier, D.; Seabaugh, A.; Banerjee, S. K.; Colombo, L. Electronics Based on Two-Dimensional Materials. *Nat. Nanotechnol.* **2014**, *9*, 768–779.
- (2) Avsar, A.; Ochoa, H.; Guinea, F.; Özyilmaz, B.; van Wees, B. J.; Vera-Marun, I. Colloquium : Spintronics in Graphene and Other Two-Dimensional Materials. *Rev. Mod. Phys.* **2020**, *92*, 021003.
- (3) Mishra, H.; Panda, J.; Maddu, R.; Sarkar, T.; Dayen, J.-F.; Belotckerkovtceva, D.; Kamalakar, M. V. Experimental Advances in Charge and Spin Transport in Chemical Vapor Deposited Graphene. *J. Phys. Mater.* **2021**, *4*, 042007.
- (4) Cummings, A. W.; Dubois, S. M.-M.; Charlier, J.-C.; Roche, S. Universal Spin Diffusion Length in Polycrystalline Graphene. *Nano Lett.* **2019**, *19*, 7418–7426.
- (5) Cummings, A. W.; Duong, D. L.; Nguyen, V. L.; Van Tuan, D.; Kotakoski, J.; Barrios Vargas, J. E.; Lee, Y. H.; Roche, S. Charge Transport in Polycrystalline Graphene: Challenges and Opportunities. *Adv. Mater.* **2014**, *26*, 5079–5094.
- (6) Dlubak, B.; Seneor, P.; Anane, A.; Barraud, C.; Deranlot, C.; Deneuve, D.; Servet, B.; Mattana, R.; Petroff, F.; Fert, A. Are Al₂O₃ and MgO Tunnel Barriers Suitable for Spin Injection in Graphene? *Appl. Phys. Lett.* **2010**, *97*, 092502.
- (7) Martin, M.-B.; Dlubak, B.; Weatherup, R. S.; Yang, H.; Deranlot, C.; Bouzehouane, K.; Petroff, F.; Anane, A.; Hofmann, S.; Robertson, J.; Fert, A.; Seneor, P. Sub-Nanometer Atomic Layer Deposition for Spintronics in Magnetic Tunnel Junctions Based on Graphene Spin-Filtering Membranes. *ACS Nano* **2014**, *8*, 7890–7895.
- (8) Feng, Y.; Trainer, D. J.; Chen, K. Graphene Tunnel Junctions with Aluminum Oxide Barrier. *J. Appl. Phys.* **2016**, *120*, 164505.
- (9) Vu, Q. A.; Kim, H.; Nguyen, V. L.; Won, U. Y.; Adhikari, S.; Kim, K.; Lee, Y. H.; Yu, W. J. A High-On/Off-Ratio Floating-Gate Memristor Array on a Flexible Substrate via CVD-Grown Large-Area 2D Layer Stacking. *Adv. Mater.* **2017**, *29*, 1703363.
- (10) Huang, Y.-J.; Lee, S. C. Graphene/h-BN Heterostructures for Vertical Architecture of RRAM Design. *Sci. Rep.* **2017**, *7*, 9679.
- (11) Dayen, J.-F.; Ray, S. J.; Karis, O.; Vera-Marun, I. J.; Kamalakar, M. V. Two-Dimensional van Der Waals Spinterfaces and Magnetic-Interfaces. *Appl. Phys. Rev.* **2020**, *7*, 011303.
- (12) Godel, F.; Venkata Kamalakar, M. V.; Doudin, B.; Henry, Y.; Halley, D.; Dayen, J.-F. Voltage-Controlled Inversion of Tunnel Magnetoresistance in Epitaxial Nickel/Graphene/MgO/Cobalt Junctions. *Appl. Phys. Lett.* **2014**, *105*, 152407.
- (13) Dlubak, B.; Martin, M.-B.; Deranlot, C.; Servet, B.; Xavier, S.; Mattana, R.; Sprinkle, M.; Berger, C.; De Heer, W. a.; Petroff, F.; Anane, A.; Seneor, P.; Fert, A. Highly Efficient Spin Transport in Epitaxial Graphene on SiC. *Nat. Phys.* **2012**, *8*, 557–561.
- (14) Han, W.; Pi, K.; McCreary, K. M.; Li, Y.; Wong, J. J. L.; Swartz, a. G.; Kawakami, R. K. Tunneling Spin Injection into Single Layer Graphene. *Phys. Rev. Lett.* **2010**, *105*, 167202.
- (15) Kamalakar, M. V.; Groenvelde, C.; Dankert, A.; Dash, S. P. Long Distance Spin Communication in Chemical Vapour Deposited Graphene. *Nat. Commun.* **2015**, *6*, 6766.
- (16) Gebeyehu, Z. M.; Parui, S.; Sierra, J. F.; Timmermans, M.; Esplandiú, M. J.; Brems, S.; Huyghebaert, C.; Garello, K.; Costache, M. V.; Valenzuela, S. O. Spin communication over 30 μm long channels of chemical vapor deposited graphene on SiO₂. *2D Mater* **2019**, *6*, 034003.
- (17) Panda, J.; Ramu, M.; Karis, O.; Sarkar, T.; Kamalakar, M. V. Ultimate Spin Currents in Commercial Chemical Vapor Deposited Graphene. *ACS Nano* **2020**, *14*, 12771–12780.
- (18) Tombros, N.; Jozsa, C.; Popinciuc, M.; Jonkman, H. T.; van Wees, B. J. Electronic Spin Transport and Spin Precession in Single Graphene Layers at Room Temperature. *Nature* **2007**, *448*, 571–574.
- (19) Popinciuc, M.; Józsa, C.; Zomer, P. J.; Tombros, N.; Veligura, A.; Jonkman, H. T.; van Wees, B. J. Electronic Spin Transport in Graphene Field-Effect Transistors. *Phys. Rev. B: Condens. Matter Mater. Phys.* **2009**, *80*, 214427.
- (20) Yamaguchi, T.; Masubuchi, S.; Iguchi, K.; Moriya, R.; Machida, T. Tunnel Spin Injection into Graphene Using Al₂O₃ Barrier Grown by Atomic Layer Deposition on Functionalized Graphene Surface. *J. Magn. Magn. Mater.* **2012**, *324*, 849–852.
- (21) Stecklein, G.; Crowell, P. A.; Li, J.; Anugrah, Y.; Su, Q.; Koester, S. J. Contact-Induced Spin Relaxation in Graphene Nonlocal Spin Valves. *Phys. Rev. Appl.* **2016**, *6*, 054015.
- (22) Anugrah, Y.; Hu, J.; Stecklein, G.; Crowell, P. A.; Koester, S. J. Independent Gate Control of Injected and Detected Spin Currents in CVD Graphene Nonlocal Spin Valves. *AIP Adv.* **2018**, *8*, 015129.
- (23) Ren, Y.; Chen, S.; Cai, W.; Zhu, Y.; Zhu, C.; Ruoff, R. S. Controlling the Electrical Transport Properties of Graphene by in Situ Metal Deposition. *Appl. Phys. Lett.* **2010**, *97*, 053107.
- (24) Giovannetti, G.; Khomyakov, P. A.; Brocks, G.; Karpan, V. M.; van den Brink, J.; Kelly, P. J. Doping Graphene with Metal Contacts. *Phys. Rev. Lett.* **2008**, *101*, 026803.
- (25) Chen, J. H.; Jang, C.; Adam, S.; Fuhrer, M. S.; Williams, E. D.; Ishigami, M. Charged-Impurity Scattering in Graphene. *Nat. Phys.* **2008**, *4*, 377–381.

- (26) Jang, C.; Adam, S.; Chen, J. H.; Williams, E. D.; Das Sarma, S.; Fuhrer, M. S. Tuning the Effective Fine Structure Constant in Graphene: Opposing Effects of Dielectric Screening on Short- and Long-Range Potential Scattering. *Phys. Rev. Lett.* **2008**, *101*, 146805.
- (27) Caridad, J. M.; Connaughton, S.; Ott, C.; Weber, H. B.; Krstić, V. An Electrical Analogy to Mie Scattering. *Nat. Commun.* **2016**, *7*, 12894.
- (28) Shi, X.; Dong, G.; Fang, M.; Wang, F.; Lin, H.; Yen, W. C.; Chan, K. S.; Chueh, Y. L.; Ho, J. C. Selective N-Type Doping in Graphene via the Aluminium Nanoparticle Decoration Approach. *J. Mater. Chem. C* **2014**, *2*, 5417–5421.
- (29) Mackenzie, D. M. A.; Galbiati, M.; De Cerio, X. D.; Sahalianov, I. Y.; Radchenko, T. M.; Sun, J.; Pena, D.; Gammelgaard, L.; Jessen, B. S.; Thomsen, J. D.; Bøggild, P.; Garcia-Lekue, A.; Camilli, L.; Caridad, J. M. Unraveling the Electronic Properties of Graphene with Substitutional Oxygen. *2D Mater* **2021**, *8*, 045035.
- (30) Childres, I.; Jauregui, L. A.; Tian, J.; Chen, Y. P. Effect of Oxygen Plasma Etching on Graphene Studied Using Raman Spectroscopy and Electronic Transport Measurements. *New J. Phys.* **2011**, *13*, 025008.
- (31) Tateno, Y.; Mitsuhashi, F.; Adachi, M.; Yonemura, T.; Saito, Y.; Yamamoto, Y.; Nakabayashi, T. An Investigation to Determine the Interface Condition between Graphene and Aluminum Oxide. *Jpn. J. Appl. Phys.* **2020**, *59*, 124001.
- (32) Zhang, L.; Koka, R. V. A Study on the Oxidation and Carbon Diffusion of TiC in Alumina-Titanium Carbide Ceramics Using XPS and Raman Spectroscopy. *Mater. Chem. Phys.* **1998**, *57*, 23–32.
- (33) Moulder, J. F.; Stickle, W. F.; Sobol, P. E.; Bomben, K. D. *Handbook of X-Ray Photoelectron Spectroscopy: A Reference Book of Standard Spectra for Identification and Interpretation of XPS Data*; Physical Electronics Division, Perkin-Elmer Corporation, 1992.
- (34) Chappé, J. M.; Fernandes, A. C.; Moura, C.; Alves, E.; Barradas, N. P.; Martin, N.; Espinós, J. P.; Vaz, F. Analysis of Multifunctional Titanium Oxycarbide Films as a Function of Oxygen Addition. *Surf. Coat. Technol.* **2012**, *206*, 2525–2534.
- (35) Ryu, S.; Liu, L.; Berciaud, S.; Yu, Y. J.; Liu, H.; Kim, P.; Flynn, G. W.; Brus, L. E. Atmospheric Oxygen Binding and Hole Doping in Deformed Graphene on a SiO₂ Substrate. *Nano Lett.* **2010**, *10*, 4944–4951.
- (36) Gammelgaard, L.; Caridad, J. M.; Cagliani, A.; Mackenzie, D. M. A.; Petersen, D. H.; Booth, T. J.; Bøggild, P. Graphene Transport Properties upon Exposure to PMMA Processing and Heat Treatments. *2D Mater.* **2014**, *1*, 035005.
- (37) Leszczynski, J. *Handbook of Computational Chemistry*; Springer Science & Business Media, 2012.
- (38) Haubner, K.; Murawski, J.; Olk, P.; Eng, L. M.; Ziegler, C.; Adolphi, B.; Jaehne, E. The Route to Functional Graphene Oxide. *ChemPhysChem* **2010**, *11*, 2131–2139.
- (39) Lesiak, B.; Kövér, L.; Tóth, J.; Zemek, J.; Jiricek, P.; Kromka, A.; Rangam, N. C Sp²/Sp³ Hybridisations in Carbon Nanomaterials – XPS and (X)AES Study. *Appl. Surf. Sci.* **2018**, *452*, 223–231.
- (40) Das, A.; Pisana, S.; Chakraborty, B.; Piscanec, S.; Saha, S. K.; Waghmare, U. V.; Novoselov, K. S.; Krishnamurthy, H. R.; Geim, A. K.; Ferrari, A. C.; Sood, A. K. Monitoring Dopants by Raman Scattering in an Electrochemically Top-Gated Graphene Transistor. *Nat. Nanotechnol.* **2008**, *3*, 210–215.
- (41) Li, X.; Cai, W.; An, J.; Kim, S.; Nah, J.; Yang, D.; Piner, R.; Velamakanni, A.; Jung, I.; Tutuc, E.; Banerjee, S. K.; Colombo, L.; Ruoff, R. S. Large-Area Synthesis of High-Quality and Uniform Graphene Films on Copper Foils. *Science* **2009**, *324*, 1312–1314.
- (42) Cançado, L. G.; Jorio, A.; Ferreira, E. H. M.; Stavale, F.; Achete, C. A.; Capaz, R. B.; Moutinho, M. V. O.; Lombardo, A.; Kulmala, T. S.; Ferrari, A. C. Quantifying Defects in Graphene via Raman Spectroscopy at Different Excitation Energies. *Nano Lett.* **2011**, *11*, 3190–3196.
- (43) Bokdam, M.; Khomyakov, P. A.; Brocks, G.; Kelly, P. J. Field Effect Doping of Graphene in Metallodielectricgraphene Hetero-

structures: A Model Based upon First-Principles Calculations. *Phys. Rev. B: Condens. Matter Mater. Phys.* **2013**, *87*, 075414.

(44) Hu, C. H.; Zheng, Y.; Zhang, Y.; Wu, S. Q.; Wen, Y. H.; Zhu, Z. Z. Electronic and Magnetic Properties of Silicon Adsorption on Graphene. *Solid State Commun.* **2011**, *151*, 1128–1130.

(45) Gillespie, P. N. O.; Martsinovich, N. Electronic Structure and Charge Transfer in the TiO₂ Rutile (110)/Graphene Composite Using Hybrid DFT Calculations. *J. Phys. Chem. C* **2017**, *121*, 4158–4171.

(46) Du, A.; Ng, Y. H.; Bell, N. J.; Zhu, Z.; Amal, R.; Smith, S. C. Hybrid Graphene/Titania Nanocomposite: Interface Charge Transfer, Hole Doping, and Sensitization for Visible Light Response. *J. Phys. Chem. Lett.* **2011**, *2*, 894–899.

(47) Castro Neto, A. H.; Guinea, F. Impurity-Induced Spin-Orbit Coupling in Graphene. *Phys. Rev. Lett.* **2009**, *103*, 026804.

(48) Santos, E. J. G.; Ayuela, A.; Sánchez-Portal, D. Universal Magnetic Properties of Sp³-Type Defects in Covalently Functionalized Graphene. *New J. Phys.* **2012**, *14*, 043022.

(49) Kochan, D.; Gmitra, M.; Fabian, J. Spin Relaxation Mechanism in Graphene: Resonant Scattering by Magnetic Impurities. *Phys. Rev. Lett.* **2014**, *112*, 116602.

(50) Wojtaszek, M.; Vera-Marun, I. J.; Maassen, T.; van Wees, B. J. Enhancement of Spin Relaxation Time in Hydrogenated Graphene Spin-Valve Devices. *Phys. Rev. B: Condens. Matter Mater. Phys.* **2013**, *87*, No. 081402(R).

(51) McCreary, K. M.; Swartz, A. G.; Han, W.; Fabian, J.; Kawakami, R. K. Magnetic Moment Formation in Graphene Detected by Scattering of Pure Spin Currents. *Phys. Rev. Lett.* **2012**, *109*, 186604.

(52) Balakrishnan, J.; Kok Wai Koon, G.; Jaiswal, M.; Castro Neto, A. H.; Özyilmaz, B. Colossal Enhancement of Spin–Orbit Coupling in Weakly Hydrogenated Graphene. *Nat. Phys.* **2013**, *9*, 284–287.

(53) Leutenantsmeyer, J. C.; Kaverzin, A. A.; Wojtaszek, M.; van Wees, B. J. Proximity Induced Room-Temperature Ferromagnetism in Graphene Probed with Spin Currents. *2D Mater.* **2016**, *4*, 014001.

Recommended by ACS

Small Polaron Hopping to Efros–Shklovskii-Like Variable Range Hopping Transition in Graphene-Wrapped V₂O₅ Nanoparticles: The Roleplay of the Mott Gap

D. Surya Bhaskaram and G. Govindaraj

DECEMBER 29, 2022

THE JOURNAL OF PHYSICAL CHEMISTRY C

READ 

Multilayer In-Plane Heterostructures Based on Transition Metal Dichalcogenides for Advanced Electronics

Hiroto Ogura, Yasumitsu Miyata, et al.

FEBRUARY 27, 2023

ACS NANO

READ 

Topological Stone–Wales Defects Enhance Bonding and Electronic Coupling at the Graphene/Metal Interface

Benedikt P. Klein, J. Michael Gottfried, et al.

AUGUST 02, 2022

ACS NANO

READ 

Artificial Graphene Nanoribbons: A Test Bed for Topology and Low-Dimensional Dirac Physics

Daniel J. Trainer, Nathan P. Guisinger, et al.

AUGUST 15, 2022

ACS NANO

READ 

Get More Suggestions >